X-ray photon correlation spectroscopy during homogenous shear flow

Wesley R. Burghardt, Marcin Sikorski, Alec R. Sandy, and Suresh Narayanan

Phys. Rev. E **85**, 021402 — Published 3 February 2012

DOI: 10.1103/PhysRevE.85.021402

X-ray Photon Correlation Spectroscopy During Homogenous Shear Flow

Wesley R. Burghardt,[1,*] Marcin Sikorski,[2] Alec R. Sandy[2] and Suresh Narayanan[2]

1. Department of Chemical and Biological Engineering, Northwestern University, Evanston, IL 60208

2. X-ray Sciences Division, Advanced Photon Source, Argonne National Laboratory, Argonne, IL 60439

- Corresponding author: w-burghardt@northwestern.edu

For submission to *Physical Review E*, August 2011
Revised, December 2011

PACS: 83.85.Hf, 82.70.Dd, 61.05.cf

Abstract

We report x-ray photon correlation spectroscopy measurements of advective and diffusive dynamics in a dispersion of colloidal particles subjected to homogeneous shear flow in a rotating disk shear cell. Intensity autocorrelation functions from scattering data collected in homodyne mode respond to the variation in velocity across the scattering volume when the scattering vector has a component parallel to the flow direction. Theoretical expressions for the impact of homogenous shear flow on the correlation function provide quantitative prediction of the dependence of correlation functions on scattering vector and shear rate. Under most circumstances, the applied shear deformation dominates the decay of the intensity correlation function. When scattering data are collected perpendicular to the flow direction it is possible to measure the diffusive dynamics of the particles free from effects of the superimposed shear flow; however, this approach will only work below some upper shear rate limit, beyond which data will be affected either by shear effects (caused by the finite width of the detector), or by particle transit through the scattering volume.

Introduction

X-ray photon correlation spectroscopy (XPCS) has emerged as a powerful tool for studying dynamic processes in colloidal [1-5] and polymeric [6-10] materials. XPCS exploits the partial coherence of x-ray beams produced at third generation synchrotron sources, resulting in 'speckle' x-ray scattering patterns characteristic of the instantaneous distribution of electron density within the sample. Time correlations of such speckle patterns are directly related to microscopic motions within the sample, usually associated with Brownian diffusion. Similar in principle to dynamic light scattering [11], XPCS may be readily used to probe opaque samples, and provides access to dynamics at smaller length scales.

While XPCS may be applied to study dynamics in diverse classes of materials, it has found widespread application to studies of soft materials in the small-angle scattering regime, probing structural dynamics on length scales of tens to hundreds of nanometers and time scales of $\sim 0.01 - 100$ seconds. This same range of scales figures prominently in the structure and rheology of many classes of complex fluids [12]. Since it enables study of microscopic dynamics in the equilibrium state, XPCS is conceptually similar to linear viscoelasticity [8,9], while offering the advantages that (i) XPCS probes structural dynamics directly rather than measuring their manifestation in the relaxation of mechanical stress; and (ii) the length scale dependence of structural dynamics may be readily assessed by performing measurements over a range of scattering vector, ($q = |\mathbf{q}| = \frac{4\pi}{\lambda}\sin\theta$; here λ is the x-ray wavelength, and 2θ is the scattering angle).

This complementarity between XPCS and rheology raises the question of whether opportunities may be afforded by a direct combination of XPCS and applied shear flow.

An ultimate goal might be to use XPCS to probe how microscopic dynamic processes change in response to flow-induced deformation or orientation of fluid microstructure in the nonlinear viscoelastic regime, similar in spirit to studies of shear-induced diffusion in dispersions of larger particles using direct real-space imaging via confocal microscopy [13]. Any such effort will be complicated by the fact that deterministic motions associated with the applied shear directly affect the measured intensity autocorrelation function measured in coherent scattering. Such effects provide the basis for one form of laser-Doppler velocimetry, where the autocorrelation function of a scattered intensity signal measured via heterodyne detection (e.g. mixing the scattered beam with a reference beam) exhibits a beat frequency directly related to the velocity of the scatterers [14]. This principle has been adapted to XPCS by Livet *et al*., who demonstrated the ability to measure extremely small velocities of filler particles in elastomers following applied deformation [15]. Conventionally, however, XPCS measurements use homodyne detection, in which case it is not the velocity itself, but rather *variation* in velocity across the scattering volume that affects the intensity autocorrelation function [16-18]. Fuller *et al*. [16] proposed and demonstrated the use of homodyne laser light scattering as a tool to measure velocity gradients in laminar flows under conditions in which the applied deformation dominates the autocorrelation function. Fluerasu and coworkers have recently applied these principles to XPCS measurements in inhomogeneous (pressure-driven) shear flows [19-21]. While Fuller *et al*. emphasized conditions in which data are dominated by the effects of shear [16], Fluerasu *et al.* have demonstrated that it is possible to perform experiments under conditions in which the native diffusive motions in the sample may be measured free from effects associated with the applied flow [19-

21]. From a rheological perspective, it is usually preferable to employ *homogenous* shear flow (that is, flows with a single, spatially uniform velocity gradient). In this paper we explore the application of XPCS during homogeneous shear flow.

Background

The theory relevant to XPCS measurements during shear is described in depth elsewhere [16-21]; here we present a brief overview of the salient points. The experimental quantity measured in XPCS is the intensity autocorrelation function:

$$g_2(\mathbf{q},t)=\frac{\left\langle I(\mathbf{q},t_0)I(\mathbf{q},t_0+t)\right\rangle_{t_0}}{\left\langle I(\mathbf{q},t_0)\right\rangle_{t_0}^2}, \tag{1}$$

computed from a time-series of intensity measurements; angled brackets denote averages over points t_0 in the series. This, in turn, is related to the intermediate scattering function $g_1(\mathbf{q},t)$ through the Siegert relationship [11]:

$$g_2(\mathbf{q},t)=1+\beta\left|g_1(\mathbf{q},t)\right|^2. \tag{2}$$

Here β is a contrast factor that depends on the coherence properties of the beam and the scattering geometry. Due to the partial coherence of synchrotron beams, this factor is generally smaller in XPCS than in dynamic light scattering. The intermediate scattering function provides fundamental information about dynamics in a sample. For instance, for a systems of N identical particles, $g_1(\mathbf{q},t)$ is given by [11]:

$$g_1(\mathbf{q},t)=\sum_{k=1}^{N}\left\langle E_k^*(0)E_k(t)\exp\left[-i\mathbf{q}\cdot(\mathbf{r}_k(0)-\mathbf{r}_k(t)\right]\right\rangle, \tag{3}$$

where $E_k(t)$ is the amplitude of scattering from particle k at time t, and $\mathbf{r}_k(t)$ is the particle's position. For the case of simple particle diffusion in a dilute suspension,

$$\left|g_1(\mathbf{q},t)\right|^2 = \exp\left[-2Dq^2t\right], \tag{4}$$

where D is the particle's Stokes-Einstein diffusivity.

For colloidal dispersions under shear, Fluerasu and coworkers show that the decay of the homodyne intensity autocorrelation function reflects three processes: particle diffusion (D), as in conventional XPCS; particle transit (T) through the scattering volume; and shear deformation (S) within the scattering volume [19]:

$$\left|g_1(\mathbf{q},t)\right|^2 = \left|g_{1,D}(\mathbf{q},t)\right|^2 \left|g_{1,T}(\mathbf{q},t)\right|^2 \left|g_{1,S}(\mathbf{q},t)\right|^2. \tag{5}$$

(This simple form in which the three contributions are factored may be justified under conditions in which the relevant time scales are widely separated [16,19].) Ackerson and Clark describe modifications to the diffusive term predicted in the presence of the applied shear flow [17]; however, under the conditions used in this work, these terms are negligible, so we simply use Eq. (4) to describe the diffusive contributions to the autocorrelation function, which involves a characteristic time $\tau_D \sim 1/Dq^2$.

The transit term arises as a result of de-correlation induced as particles enter and leave the scattering volume. It produces decay of the correlation function over a characteristic time $\tau_T \sim w/V$, where w is the beam width and V is a characteristic velocity, here taken to be the velocity of the moving plate in the homogeneous shear flow (Figure 1). The detailed functional form for $\left|g_{1,T}(\mathbf{q},t)\right|^2$ will depend on the intensity profile across the beam [19]. As discussed below, however, transit time effects should be negligible under the conditions used here.

Steady flow will make a predictable contribution to the relationships among particle positions in Eq. (3) as time elapses [19]. X-rays scattered from moving particles

are Doppler-shifted; a pair of particles with a difference in velocity, $\delta\mathbf{v}$, will produce a beat frequency $\mathbf{q}\cdot\delta\mathbf{v}$ when their scattered x-rays interfere at the detector. The shear contribution to the correlation function is computed by averaging this effect for all pairs of particles in the scattering volume. We consider shear flow as illustrated in Figure 1:

$$v_x = \frac{V}{H}y = \dot{\gamma}y; \quad v_y = v_z = 0 \tag{6}$$

In this geometry, $\mathbf{q}\cdot\delta\mathbf{v} = q_x\dot{\gamma}\delta y$, where δy is the displacement between a pair of particles along the *y*-direction. For large *N*, the sum over all particle pairs may be represented as a double integral over the scattering volume. Since velocity only varies in the *y*-direction for the flow under consideration here, integration is only required in this direction, leading to [18,19]:

$$\left|g_{1,S}(\mathbf{q},t)\right|^2 = \frac{1}{H^2}\int_0^H\int_0^H \cos(q_x\dot{\gamma}(y_2-y_1)t)dy_1dy_2 = \frac{\sin^2\left(q_x\dot{\gamma}Ht/2\right)}{\left(q_x\dot{\gamma}Ht/2\right)^2}. \tag{7}$$

Fluerasu and coworkers derived and applied a more complicated expression appropriate for parabolic velocity distributions associated with pressure-driven laminar flows; the relative simplicity of Eq. (7) is another advantage of the homogeneous flow employed here. Neglecting transit effects, the final expression governing intensity correlation functions measured in homogeneous shear flow is:

$$g_2(\mathbf{q},t) = 1+\beta\exp\left[-2Dq^2t\right]\frac{\sin^2\left(q_x\dot{\gamma}Ht/2\right)}{\left(q_x\dot{\gamma}Ht/2\right)^2} \tag{8}$$

Experimental Methods

An aqueous dispersion of charge-stabilized polystyrene particles with nominal diameter of 100 nm (Duke Scientific) was dispersed in glycerol, and the water removed

by vacuum drying. Due to uncertainty in the concentration of the parent aqueous PS latex, the particle loading could not be controlled precisely; scattering data presented below suggest a particle volume fraction of approximately 0.12. X-ray scattering experiments were performed at beam line 8ID-I of the Advanced Photon Source, using a 20 x 20 μm x-ray beam of energy 7.35 keV. Static small-angle x-ray scattering (SAXS) data were collected using direct detection with a PI LCX-1300 charge-coupled device (CCD) detector. XPCS experiments were performed using a faster SMD 1M60 CCD detector, again using direct detection of x-rays. To maximize time resolution, data were collected using a region of interest 128 pixels tall and 1024 pixels wide on the CCD, leading to an image acquisition rate of 330 frames per second. XPCS data were collected in sequences of 2048 data frames. Within each sequence, intensity autocorrelation functions are computed for each pixel, and then averaged over 'bins' defining the desired q_x and q_z values (described below) to improve signal to noise. Further noise reduction is achieved by averaging correlation functions computed using a large number (between 60 and 90) of data sequences obtained under identical conditions. Applied shear flow helps mitigate concerns of radiation-induced sample damage, but as a precaution the shear cell was displaced slightly between successive sequences to avoid prolonged illumination of the same spot.

Due to the influence of shear flow, the decay of the autocorrelation function is predicted to be anisotropic. To test predictions of Eq. (8), experiments were performed using two different detector positions and associated pixel binning schemes (Figure 1). In position 1, the active area of the detector was aligned symmetrically along the flow direction, such that $q \approx q_x$. Separate experiments were conducted in position 2, where

the detector was oriented parallel to, but displaced away from the q_x axis. Here, smaller pixel bins were used allowing q_x and q_z to be independently varied. Bins were arranged such that data collected for positive and negative q_x values of equal magnitude could be compared, and to allow analysis of data collected at locations along the q_z axis ($q_x \approx 0$), where it should be possible to measure diffusive dynamics free from the influence of the applied shear [19].

Shear flow was produced using a rotating disk shear cell that, locally, produces the flow illustrated in Figure 1. In this shear cell, thin Kapton® windows are glued to aluminum supporting surfaces. The fixed support plate has a small aperture, while the moving plate has three slots arranged circumferentially to allow transmission of x-rays as the shear cell rotates. The sample thickness, H, in these studies was 0.8 mm. Shear cell rotation was driven through a timing belt by a microstepping motor operating at a resolution of 50,000 steps per revolution. To provide smooth motion at the low shear rates employed here, a 20:1 gear reducer was used; further reduction by a factor of 2.5 was imparted by the sizing of timing belt pulleys on the shear cell and motor. Even with these precautions, the discrete nature of the applied motion is still a potential concern. Further discussion in the Supplemental Material for this paper [24] suggests that its impact should be negligible in these experiments.

Results

Static SAXS data on the polystyrene latex dispersion in glycerol exhibit behavior typical of moderately concentrated dispersions of monodisperse colloids (Figure 2). Data were well described by a scattering model with a hard-sphere structure factor and a

spherical particle form factor modified to account for polydispersity. XPCS experiments were restricted to relatively small q, where the sample scattered most strongly, and where the dynamics were sufficiently slow to resolve. Correlation function data obtained under quiescent conditions were fit well by the single exponential function of Eq. (4) (Figure 3(a)). Diffusivity values extracted from the curve fits show a weak dependence on scattering vector (Figure 3(b)). Comparison of diffusivity against the static structure factor suggests that this q-dependence arises from 'de Gennes narrowing' where dynamics are slowed at length scales associated with structure factor peaks [2].

Over the q-range studied here, the characteristic diffusive time scale τ_D ranges from 0.05 to 0.33 seconds. Conversely, over the shear rate range 0.001 to 0.02 s^{-1}, the transit time τ_T ranges from 1.25 – 25 seconds. Since this is large compared to τ_D, the neglect of transit time effects in Eq. (8) is justified. In fact, in the experiments reported here, shear effects will always dominate over transit time effects. The characteristic time scale for shear, $\tau_S \sim 1/q_x\dot{\gamma}H = 1/q_xV$; hence the ratio of shear to transit time scales is given by:

$$\frac{\tau_S}{\tau_T} \sim \frac{1}{wq_x}. \qquad (9)$$

This ratio will be small except for *extremely* small q_x values, where $q_x \sim 1/w$ (for a beam of width 20 μm, this requires $q_x \sim 5 \times 10^{-6}$ $Å^{-1}$). Thus, during shear flow, the impact of the shear term will dominate over the transit term in Eq. (5).

Application of shear flow dramatically accelerates the decay and changes the shape of the correlation function (Figure 4). After fitting the diffusivity to the quiescent data, there are no remaining fitting parameters in Eq. (8); solid lines in Figure 4 represent

true predictions, which quantitatively describe both shear rate and q_x-dependencies of the correlation function (further examples of data and predictions are provided in Supplemental Material [24]). At the lowest shear rate used in Figure 4, slight deviations appear between data and predictions. At low rates, the characteristic diffusion and shear times become comparable, which may undermine the separation of time scales required for the factorability present in Eq. (5).

Eq. (8) continues to describe data well for detector position 2, in which q and q_x are no longer equivalent (Figure 5). While the diffusive term depends on the full magnitude of **q**, the shear term depends only on the component of **q** along the flow direction. Data collected for positive and negative q_x values of equal magnitude are in excellent agreement, and are well described by Eq. (8) (Figure 5(c) & (d)). This lateral positioning of the detector also allows experiments perpendicular to the flow direction ($q_x = 0$), where Eq. (8) predicts no effect of the applied shear flow (Figure 5(a)). Up to a shear rate of 0.01 s^{-1} the measured correlation functions are, indeed, indistinguishable to within experimental error. However, at the highest shear rate of 0.02 s^{-1}, the correlation function decay is visibly accelerated. This is attributed to the finite width of the pixel bin used to average correlation functions in this position (Figure 1), which leads to contributions to the averaged correlation function from detector positions with finite $|q_x|$, allowing shear effects to 'leak' into the measurement. To illustrate this, the dashed line in Figure 5(a) presents the prediction of Eq. (8) using a 'representative' value of q_x (taken to be the average of $|q_x|$ across the bin), which is found to capture the accelerated time scale reasonably well. While a crude simplification, this calculation demonstrates that, even at locations perpendicular to the flow direction, shear effects will impede

measurements of diffusive dynamics unless either shear rate or the range of $|q_x|$ sampled by the detector is kept sufficiently small. Fluerasu and coworkers have examined this question in detail, and report diagrams of parameter space for which diffusive dynamics may be measured during shear flow [19-21]. (Measurements conducted in a second 'row' of pixel bins for this lateral detector position show qualitatively the same behavior; additional data are presented in Supplemental Material [24].)

Discussion

Results presented above demonstrate the feasibility of XPCS measurements in homogeneous shear, and confirm that the impact of shear of the measured intensity correlation function is reliably predictable. From a rheological perspective, the shear rate range studied here is limited to rather low values; even slow shear flows have a dramatic effect on the correlation time. This limitation arises in part due to the limited data acquisition rate possible when measuring XPCS correlation functions using CCD-based area detectors. It is possible to measure much faster dynamics using point detectors and conventional hardware correlators, but loss of the signal average afforded by large numbers of (approximately) equivalent pixels in an area detector would limit such measurements to very strongly scattering samples.

The high sensitivity to shear gradients also means that measurements of the intrinsic diffusive dynamics of the sample (i.e. measuring correlation functions using data collected in the q_z direction, perpendicular to the flow) are possible only at fairly low shear rates. This problem may, in principle, be managed by increasingly narrow definition of the detector area so as to limit $|q_x|$. Drawing on Eq. (10), the best that can be

done in this vein is to reduce $|q_x|$ to the point where $\tau_S \sim \tau_T$, beyond this, the transit term becomes the limiting factor. Reaching this condition would, however, require restriction to an extraordinary sharply defined band of reciprocal space along the q_z direction. In our experiments, for instance, an increment of $q \sim 1/w = 5 \times 10^{-6}$ Å^{-1} corresponds to less than the width of a single pixel on the CCD detector. Even if this condition were satisfied, the presence of the transit term dictates that 'clean' measurements of a sample's diffusive dynamics would require that:

$$\tau_D \le \tau_T \quad \Rightarrow \quad \tau_D \le \frac{w}{\dot{\gamma} H} \quad \Rightarrow \quad \tau_D \dot{\gamma} \le \frac{w}{H}. \tag{10}$$

In the shear flow geometry employed here, $w/H << 1$, and Eq. (10) represents a strong restriction on the strength of the applied flow for which it is possible to measure diffusive dynamics under shear. The requirement that $\tau_D \dot{\gamma} << 1$ means that flow will generally be too weak to significantly perturb the underlying structure or microscopic dynamics. For instance, in the experiments reported here the maximum Peclet number ($Pe = \dot{\gamma} a^2 / D$, a = particle radius) is about 0.007. In this geometry, then, it appears that only measurements of essentially equilibrium dynamics are possible in the presence of shear flow. Of course even this fact may be beneficial in a practical setting where shear flow may be used as a strategy to mitigate beam damage of a sensitive sample [19].

It is instructive to consider alternate experimental arrangements that may offer improved opportunities for XPCS during shear. The characteristic shear time is determined by the dimension of the scattering volume in the direction of the velocity gradient [16]. In the geometry used in this work (Figure 1), the long dimension of the scattering volume (H) points along the velocity gradient, which contributes to the short

correlation times observed at even modest shear rates. Figure 6 presents a possible alternative configuration, in which the incident (narrow) beam passes 'sideways' (along the *z*-direction) through a homogenous shear flow. In this case, the dimension of the scattering volume in the gradient direction is much smaller, such that $\tau_S \sim 1/q_x\dot{\gamma}w$ rather than $1/q_x\dot{\gamma}H$. Such an arrangement would facilitate measurements of correlation functions under shear over a wider range of rates than is possible using the configuration of Figure 1. Further, if one wished to use the intrinsic capability of homodyne XPCS to measure velocity gradients in complex flow situations such as shear banding [22], this arrangement would offer advantages. The concept shown in Figure 6 does, however, present new challenges. Any parasitic velocity gradients along the beam direction would likely dominate the autocorrelation function due to the longer dimension of the scattering volume in this direction. It would thus be necessary to maintain zero-stress free surfaces at the sides of the flow. A second issue is that the mathematical form of the shear autocorrelation function in this scenario would depend on the lateral intensity distribution in the beam, making quantitative work more difficult [16]. While higher shear rates may be possible with this arrangement, an analysis analogous to that presented above leads to the conclusion that, in a 'best case' scenario, constraints on measuring diffusive dynamics free from directly influence of the applied flow will require that $\tau_D\dot{\gamma} \leq 1$. While this is an improvement over Eq. (10), it still indicates that opportunities to use XPCS to monitor microscopic dynamics in a sample that has been pushed far from its equilibrium state by applied shear are limited. Despite these limitations, there are other ways in which the intersection of applied shear flow and XPCS can offer fruitful avenues of inquiry. For instance, XPCS may be used to study the time evolution of structural dynamics in

complex fluids that have been perturbed far from equilibrium by prior flow [3]. In addition, the combination of XPCS with other modes of shear flow, such as oscillatory shear or step-strain, may offer opportunities to probe strain-dependent phenomena in various complex fluids. For instance, the dynamic light scattering 'echo' technique employed by Petekidis *et al.* [23] could be adapted to XPCS.

Conclusions

XPCS has been successfully implemented to measure advective and diffusive dynamics in a colloidal dispersion during homogeneous shear flow. Even at modest deformation rates, the applied shear deformation dominates decay of the intensity autocorrelation function under most conditions; these effects may be quantitatively predicted by relevant theories. When scattering data are measured perpendicular to the flow direction, it is possible to measure the diffusive dynamics of the colloidal particles free from interference from the effects of the applied flow. Even for data measured in this configuration, however, the finite width of pixel bins on the detector result in shear effects on correlation functions measured at higher rates, due to the inclusion of detector pixels with a small component of **q** parallel to the flow direction. Transit of particles through the scattering volume can also affect correlation functions measured in the perpendicular direction, although under most circumstances shear effects will dominate over transit effects. These factors place limits on the strength of the flow for which measurements of purely microscopic dynamics are possible; in particular, it appears unlikely that XPCS measurements during shear can access conditions under which flow strongly perturbs the fluid structure away from its equilibrium state.

Acknowledgments

Experiments were performed at beamline 8ID-I of the Advanced Photon Source. Use of the Advanced Photon Source, an Office of Science User Facility operated for the U.S. Department of Energy (DOE) Office of Science by Argonne National Laboratory, was supported by the U.S. DOE under Contract No. DE-AC02-06CH11357. We acknowledge helpful assistance from Mr. Ray Ziegler, and the X-ray Sciences Division Visitor Program at Argonne National Laboratory.

References

1. S. B. Dierker, R. Pindak, R. M. Fleming, I. K Robinson and L. Berman, Phys. Rev. Lett. **75**, 449 (1995).
2. L. B. Lurio et al. Phys. Rev. Lett. **84**, 785 (2000).
3. B. Chung, S. Ramakrishnan, R. Bandyopadhyay, D. Liang, C. F. Zukoski, J. L. Harden and R. L. Leheny, Phys. Rev. Lett. **96**, 228301 (2006).
4. X. Lu, S. G. J. Mochrie, S. Narayanan, A. R. Sandy and M. R. Sprung, Soft Matter **6**, 6160 (2010).
5. M. Sikorski, A. R. Sandy and S. Narayanan, Phys. Rev. Lett. **106**, 188301 (2011).
6. P. Falus, M. A. Borthwick and S. G. J. Mochrie, Phys. Rev. Lett. **94**, 016105 (2005).
7. M. L. Ruegg, A. J. Patel, S. Narayanan, A. R. Sandy, S. G. J. Mochrie, H. Watanabe and N. P. Balsara, Macromolecules **39**, 8822 (2006).
8. A. J. Patel, S. Narayanan, A. Sandy, S. G. J. Mochrie, B. A. Garetz, H. Watanabe and N. P. Balsara, Phys. Rev. Lett. **96**, 257801 (2006).
9. K. L. Brinker, S. G. J. Mochrie and W. R. Burghardt, Macromolecules **40**, 5150 (2007).
10. A. J. Patel, S. Mochrie, S. Narayanan, A. Sandy, H. Watanabe and N. P. Balsara, Macromolecules **43**, 1515 (2010).
11. B. J. Berne and R. Pecora, *Dynamic Light Scattering with Applications to Chemistry, Biology and Physics* (Wiley, New York, 1976).
12. R. G. Larson, *The Structure and Rheology of Complex Fluids* (Oxford, New York, 1998).

13. R. Besseling, E. R. Weeks, A. B. Schofield and W. C. K. Poon, Phys. Rev. Lett. **99**, 028301 (2007).

14. F. Durst, A. Melling and J. H. Whitelaw, *Principles and Practice of Laser-Doppler Anemometry* (Academic, New York, 1976).

15. F. Livet, F. Bley, F. Ehrburger-Dolle, I. Morfin, E. Geissler and M. Sutton, J. Synch. Rad. **13**, 453 (2006).

16. G. G. Fuller, J. M. Rallison, R. L. Schmidt and L. G. Leal, J. Fluid Mech. **100**, 555 (1980).

17. B. J. Ackerson and N. A. Clark, J. Phys. (Paris) **42**, 929 (1981).

18. T. Narayanan, C. Cheung, P. Tong, W. I. Goldburg and X.-I. Wu, Appl. Optics, **36**, 7639 (1997).

19. S. Busch, T. H. Jensen, Y. Chushkin and A. Fluerasu, Eur. Phys. J. E **26**, 55 (2008).

20. A. Fluerasu, A. Moussaïd, P. Falus, H. Gleyzolle and A. Madsen, J. Synch. Rad. **15**, 378 (2008).

21. A. Fluerasu, P. Kwasniewski, C. Caronna, F. Destremaut, J.-B. Salmon and A. Madsen, New J. Phys. **12**, 035023 (2010).

22. Y. T. Hu, C. Palla and A. Lips, J. Rheol. **52**, 379 (2008).

23. G. Petekidis, A. Moussaïd and P. N. Pusey, Phys. Rev. E **66**, 051402 (2002).

24. See Supplemental Material at [URL to be inserted by publisher] for additional discussion of the impact of discrete shear cell motion on autocorrelation functions, and for additional data Figures.

Figure Headings

Figure 1. Diagram of experiment, illustrating coordinates used to define applied shear flow field, and showing the two different positions and binning schemes used for XPCS data acquisition during shear flow. The gray circle has a radius of $q = 0.0082$ Å^{-1}, the location of the first form factor minimum of the colloidal dispersion of polystyrene latex particles used as a sample in this work.

Figure 2. Static small-angle x-ray scattering from the polystyrene latex particle dispersion. The data were fit to a form factor/structure factor model for polydisperse spherical particles, using the following parameters: mean particle radius = 54.6 nm; distribution breadth = 5.5 nm (FWHM); particle volume fraction = 0.12.

Figure 3. Dynamics of polystyrene latex particle dispersion in quiescent state. (a) Intensity autocorrelation function measured at $q = 0.00154$ (●), 0.00215 (Δ), 0.00279 (■), 0.00343 (◇), 0.00413 (▼) and 0.00480 Å^{-1} (×). Data were measured at detector position #1 (Fig. 1). Solid lines represent single-exponential fits using Eq. (4). (b) Diffusivity as a function of scattering vector, overlayed with a plot of structure factor, $S(q)$ determined from the model fit to the data in Fig. 2.

Figure 4. Intensity autocorrelation functions measured in polystyrene latex particle dispersion during shear using detector position #1 ($q_z \approx 0$; Fig. 1), at (a) $q \approx q_x = 0.00215$ and (b) $q \approx q_x = 0.00413$ Å^{-1}. Applied shear rate: 0 (●), 0.002 (Δ), 0.005 (■), 0.01 (◇)

and 0.02 s^{-1} (▼). Solid curves are predictions of Eq. (8), using D = 9430 and 6520 nm^2/s in parts (a), and (b), respectively.

Figure 5. Intensity autocorrelation functions measured in polystyrene latex particle dispersion during shear using detector position #2 (Fig. 1), at (a) q_z = 0.0017, $|q_x|$ = 0; (b) q_z = 0.0017, $|q_x|$ = 0.0012; and (c) q_z = 0.0017, $|q_x|$ = 0.0024 $Å^{-1}$. Applied shear rate: 0 (●,○), 0.003 (▲,Δ), 0.007 (■,□), 0.01 (◆,◇) and 0.02 s^{-1} (▼,▽). Open and closed symbols in parts (b) and (c) represent data collected for positive and negative values of q_x. Solid curves in parts (b) and (c) are predictions of Eq. (8), using, respectively, D = 11,200 and 7440 nm^2/s. Dashed curve in part (a) represents predictions of Eq. (8) using D = 15,400 nm^2/s, and a representative value of $|q_x|$ = 0.00015 $Å^{-1}$.

Figure 6. Schematic of possible alternate configuration for XPCS measurements during shear. Here the beam width, w, determines the characteristic correlation time associated with shear: $\tau_S \sim 1/q_x \dot{\gamma} w$.

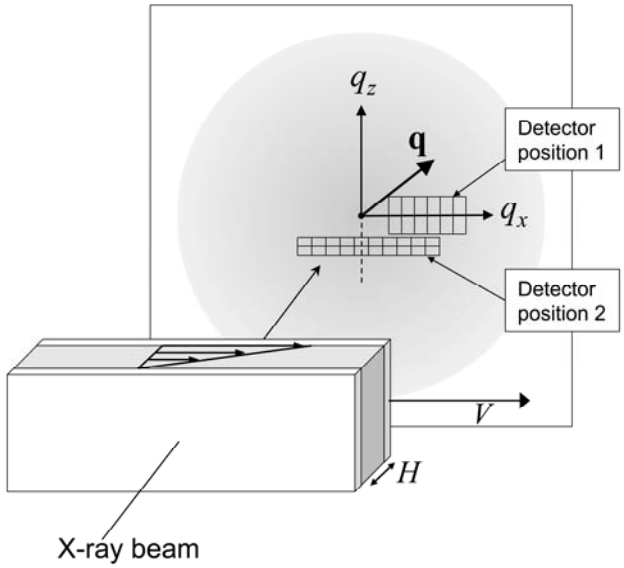

Figure 1. Diagram of experiment, illustrating coordinates used to define applied shear flow field, and showing the two different positions and binning schemes used for XPCS data acquisition during shear flow. The gray circle has a radius of $q = 0.0082$ Å^{-1}, the location of the first form factor minimum of the colloidal polystyrene particle dispersion used as a sample in this work.

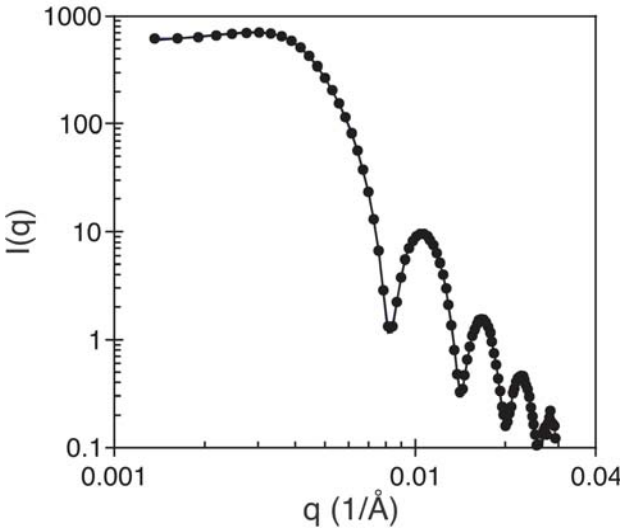

Figure 2. Static small-angle x-ray scattering from the polystyrene latex particle dispersion. The data were fit to a form factor/structure factor model for polydisperse spherical particles, using the following parameters: mean particle radius = 54.6 nm; distribution breadth = 5.5 nm (FWHM); particle volume fraction = 0.12.

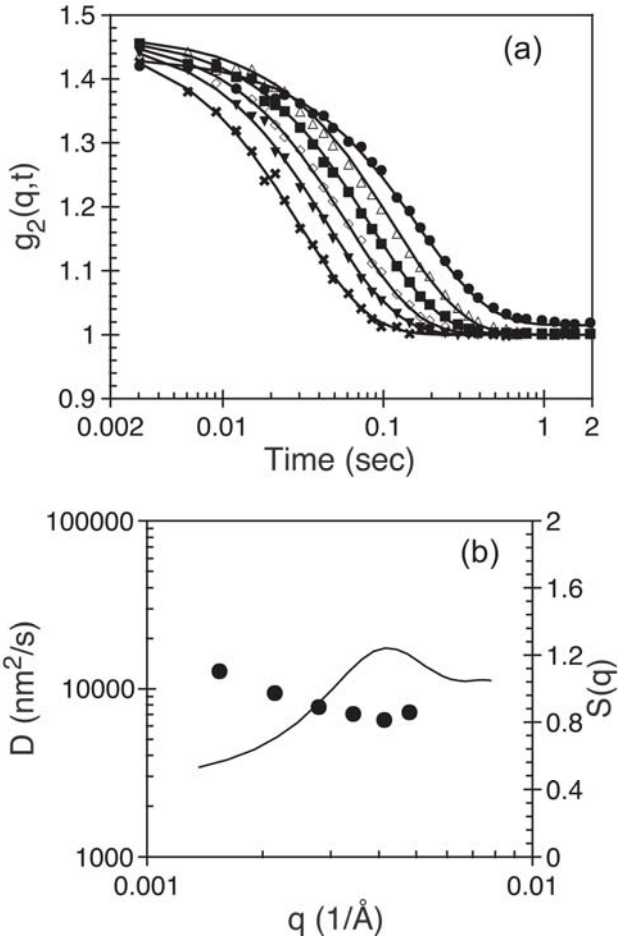

Figure 3. Dynamics of polystyrene latex particle dispersion in quiescent state. (a) Intensity autocorrelation function measured at q = 0.00154 (●), 0.00215 (Δ), 0.00279 (■), 0.00343 (◇), 0.00413 (▼) and 0.00480 $Å^{-1}$ (×). Data were measured at detector position 1 (Fig. 1). Solid lines represent single-exponential fits using Eq. (4). (b) Diffusivity as a function of scattering vector, overlayed with a plot of structure factor, $S(q)$ determined from the model fit to the data in Fig. 2.

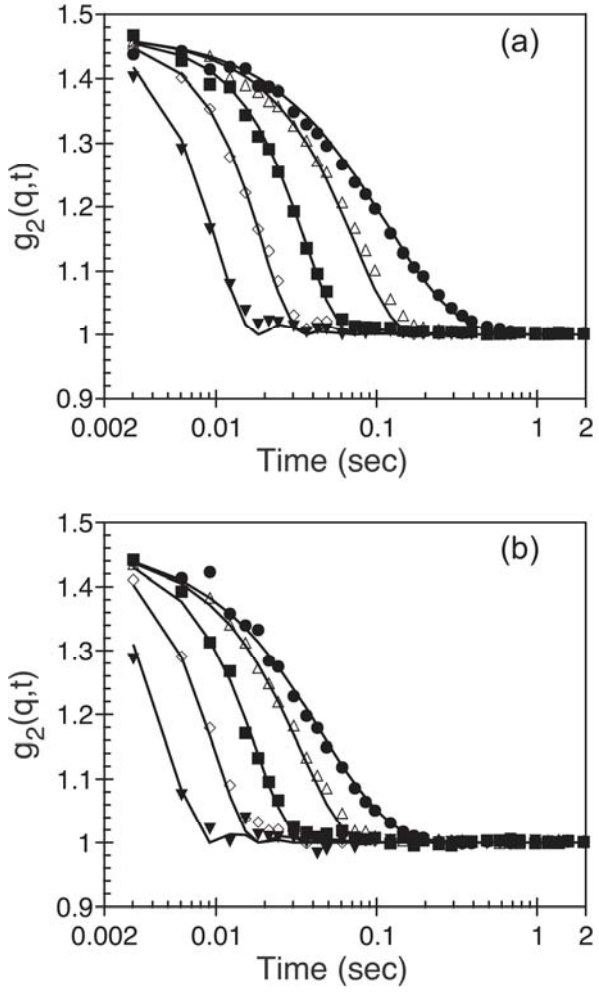

Figure 4. Intensity autocorrelation functions measured in polystyrene latex particle dispersion during shear using detector position 1 ($q_z \approx 0$; Fig. 1), at (a) $q \approx q_x = 0.00215$ and (b) $q \approx q_x = 0.00413$ Å^{-1}. Applied shear rate: 0 (●), 0.002 (Δ), 0.005 (■), 0.01 (◇) and 0.02 s^{-1} (▼). Solid curves are predictions of Eq. (8), using $D = 9430$ and 6520 nm^2/s in parts (a), and (b), respectively.

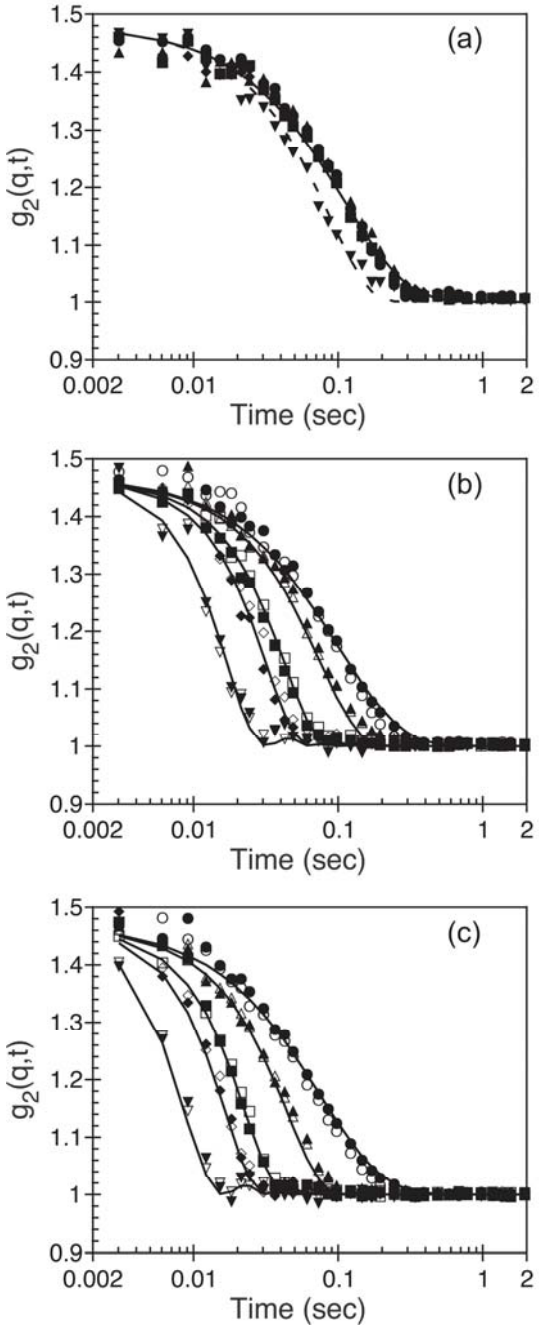

Figure 5. Intensity autocorrelation functions measured in polystyrene latex particle dispersion during shear using detector position 2 (Fig. 1), at (a) $q_z = 0.0017$, $|q_x| = 0$; (b) $q_z = 0.0017$, $|q_x| = 0.0012$; and (c) $q_z = 0.0017$, $|q_x| = 0.0024$ Å^{-1}. Applied shear rate: 0 (●,○), 0.003 (▲,Δ), 0.007 (■,□), 0.01 (◆,◇) and 0.02 s^{-1} (▼,▽). Open and closed symbols in parts (b) and (c) represent data collected for positive and negative values of q_x. Solid curves in parts (b) and (c) are predictions of Eq. (8), using, respectively, D = 11,200 and 7440 nm^2/s. Dashed curve in part (a) represents predictions of Eq. (8) using D = 15,400 nm^2/s, and a representative value of $|q_x| = 0.00015$ Å^{-1}.

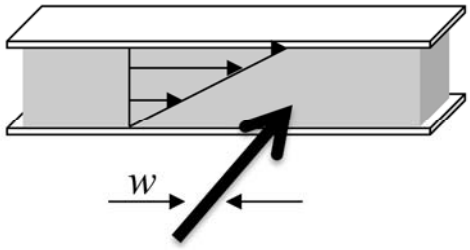

Figure 6. Schematic of possible alternate configuration for XPCS measurements during shear. Here the beam width, w, determines the characteristic correlation time associated with shear: $\tau_S \sim 1/q_x\dot{\gamma}w$.